

Chapter 9

Spin Codes



Vahid Ranjbar

Abstract This chapter reviews the approaches to numerically integrate the spin-orbit and how they are applied in several spin codes.

9.1 Overview of Codes

Along with theoretical developments and polarized beam studies at the weak focusing synchrotron ZGS (polarized proton beams were produced from 1973) and at the strong focusing synchrotron Saturne 2 (proton and light ion beams, from 1981), a number of spin tracking techniques have been devised over the years along with the design and operation of polarized beam facilities.

Early computer codes were based on matrix transport techniques, two early instances were lattice design and spin dynamics studies for polarized ion beams at Saturne 2 and its synchrotron injector Mimas [1], for electron beams accounting for synchrotron radiation at SPEAR [2]. Numerical integration of the equations of motion was later resorted to and allowed solving spin motion in arbitrary fields, and to high order in particle coordinates, so allowing accurate treatment of spin motion in special devices such as snakes and in field maps [3, 4]. With the increased interest in polarized beams and the design and construction of accelerator facilities, a number of analytical methods have been developed and used in spin codes.

This manuscript has been authored by Brookhaven Science Associates, LLC under Contract No. DE-SC0012704 with the U.S. Department of Energy. The United States Government and the publisher, by accepting the article for publication, acknowledges that the United States Government retains a non-exclusive, paid-up, irrevocable, world-wide license to publish or reproduce the published form of this manuscript, or allow others to do so, for United States Government purposes.

V. Ranjbar (✉)
Electron-Ion Collider, Brookhaven National Laboratory, Upton, NY, USA
e-mail: vranjbar@bnl.gov

This is a U.S. government work and not under copyright protection in the U.S.;
foreign copyright protection may apply 2023
F. Méot et al. (eds.), *Polarized Beam Dynamics and Instrumentation*
in *Particle Accelerators*, Particle Acceleration and Detection,
https://doi.org/10.1007/978-3-031-16715-7_9

Indications regarding possible spin dynamics capabilities of existing beam optics codes may be found in accelerator codes repositories [5, 6].

There are several direct spin-orbit tracking codes freely obtainable at the time of this writing. These can be categorized based on their method of numerical integration, order of accuracy, and also their inclusion of radiative effects necessary when considering electron spin tracking.

- **Bmad** [7] is a Fortran 2008 platform which can make use of several different spin-orbit tracking algorithms. These include Runge-Kutta style and Symplectic PTC style orbit integrators. It reads lattices written using MAD like syntax and can be run exploiting multi-threading with certain restrictions. It is well documented and maintained. It has recently been used to help model several of the future Electron-Ion Collider lattices including the Electron Storage Ring and the Rapid Cycling Synchrotron.
- **COSY Infinity** [8] uses a differential algebraic method to generate transfer maps for both orbit and spin. It accomplishes this by generating derivatives to arbitrary order using automatic differentiation [9]. It includes higher-order nonlinearities, normal form analysis, and symplectic tracking. It has been used for instance to support Electric Dipole Moment lattice simulations at COSY [10].
- **GPUSPINTRACK**: a symplectic drift-kick, bend-kick and matrix-kick integrator [11] (see Sect. 9.5).
- **SITROS** [12] was used at the HERA e-p collider, it was developed in the early 1980s by Jorg Kewisch and updated in the 1990s and early 2000s. It tracks a group of electrons or positrons through the lattice and applies radiative kicks using a Monte-Carlo style algorithm to simulate the radiative effects on longitudinal dynamics and spin. It first performs orbital tracking to generate an equilibrium phase space distribution, later spin tracking is included. To speed up the tracking time transfer maps are developed for whole sections of the ring instead of tracking element by element. It is used today to model aspects of the spin dynamics and compute polarization life-time in the EIC Electron Storage Ring [13].
- **SPINK**: a symplectic kick based first order integrator [14] (see Sect. 9.4).
- **SPRINT** performs multi-turn spin-orbit tracking for linearized orbital motion, but fully nonlinear spin motion and all orders of resonance [15].
- **Zgoubi**: Taylor based integrator, handles \mathbf{E} and \mathbf{B} fields, includes radiative effects. Degree of non-symplecticity inherent to truncated Taylor series is mostly controlled by the integration step size [16] (see Sect. 9.3).

Then there are several reduced spin tracking codes which integrate a reduced form the T-BMT equation. These include the codes **SLIM** [2, 17] and **T-BMT** [18].

In addition to direct spin-orbit tracking codes there are codes which calculate the spin resonances for a given energy range based on the optics for an accelerator lattice. These include **DEPOL** [19], **ASPIRRIN** [20] and **SPRINT** [21].

To illustrate the general approaches for numerical integration, we explore the three codes **Zgoubi**, **SPINK** and **GPUSPINTRACK** in more detail in the following sections. **DEPOL** and **T-BMT** are also addressed in dedicated sections.

9.2 Integration of the Spin and Orbit

As we learned in previous chapters the dynamics of the spin vector of a charged particle in the laboratory frame is described by the T-BMT equation,

$$\frac{d\mathbf{S}}{dt} = \frac{q}{\gamma m} \mathbf{S} \times \left((1 + G\gamma)\mathbf{B}_\perp + (1 + G)\mathbf{B}_\parallel + \left(\frac{1}{\gamma + 1} + G \right) \gamma \frac{\mathbf{E} \times \boldsymbol{\beta}}{c} \right) \quad (9.1)$$

\mathbf{S} is the spin vector in the rest frame of the particle, \mathbf{E} and \mathbf{B} are fields in the laboratory, the magnetic field components \mathbf{B}_\perp and \mathbf{B}_\parallel are defined with respect to the particle's velocity. $G = \frac{g-2}{2}$ is the anomalous magnetic moment coefficient which for protons is 1.7928474, and γmc^2 is the energy of the particle. We can transform this equation by expanding about a reference orbit described by a Frénet-Serret coordinate system. See Fig. 9.1. Thus we have

$$\frac{d\hat{x}}{ds} = \frac{\hat{s}}{\rho}, \quad \frac{d\hat{s}}{ds} = -\frac{\hat{x}}{\rho}, \quad \text{and} \quad \frac{d\hat{z}}{ds} = 0, \quad (9.2)$$

Particle motion can be parameterized in this coordinate system as

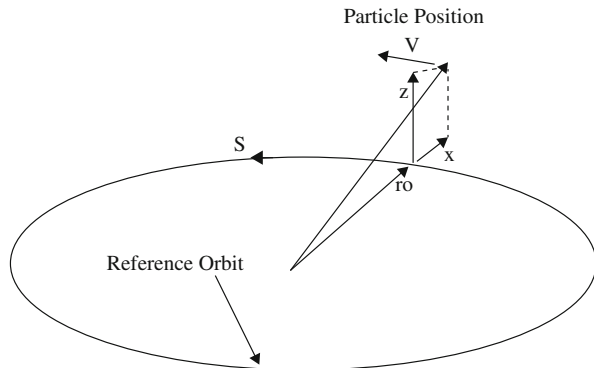
$$\mathbf{r} = \mathbf{r}_0(s) + x\hat{x} + z\hat{z}, \quad (9.3)$$

where $\mathbf{r}_0(s)$ is the reference orbit, and $\hat{s} = d\mathbf{r}_0/ds$.

The integration of the T-BMT equation requires the knowledge of the spatial dependence of the fields, which in turn depend on the trajectory of the charged particle in the optical elements. A particle traversing a quadrupole magnet off axis will experience a different magnetic field than one going through the center. We calculate this trajectory by integrating the Lorentz force equation.

$$\frac{d\mathbf{p}}{dt} = q (\mathbf{E} + \mathbf{v} \times \mathbf{B}) \quad (9.4)$$

Fig. 9.1 The curvilinear coordinate system for particle motion in a circular accelerator. The unit vectors \hat{x} , \hat{s} and \hat{z} are the transverse radial, longitudinal, and transverse vertical basis vectors; and $\mathbf{r}_0(s)$ is the reference orbit



This is the job which all accelerator codes need to accomplish and to do this they use several standard approaches:

- Non-symplectic approaches. They typically use a Runge-Kutta type algorithm or a ray tracing method which use the mechanics of a Taylor expansion of the equations of motion.
- Symplectic Methods. These include both thin lens-kick and thick lens integrators.

9.3 Zgoubi

Step-wise ray-tracing has accompanied accelerator design concurrently with the emergence of computers and magnetic field simulations in the early 1950s, with Runge-Kutta being one of the early methods [22]. Step-wise integration of the orbital motion allows the necessary accuracy for solving the Thomas-BMT differential equation. This is especially important in small rings where lattice optics field perturbations matter, and in beam transport lines which may include special magnets and fancy spin manipulations; these were the main reasons why step-wise spin tracking were developed in the late 1980s in Zgoubi (originally a spectrometer code) in the context of partial snake plans at Saturne [3], and in Raytrace [23] (a spectrometer code as well) at the AGS for polarized beam transport in AGS and RHIC facility transfer lines [4]. A serendipity of step-wise integration is its yielding 6D motion ab initio as it handles the three components of the position and velocity vectors, independently.

Zgoubi has been in use since the early 2000s at RHIC [24] and its injectors [25, 26], and at present for spin simulations in the EIC electron machines [27, 28]. Preservation of motion invariants, in relation with the truncated Taylor series integration method, is controlled over millions of turns in RHIC size EIC rings, via step size mostly.

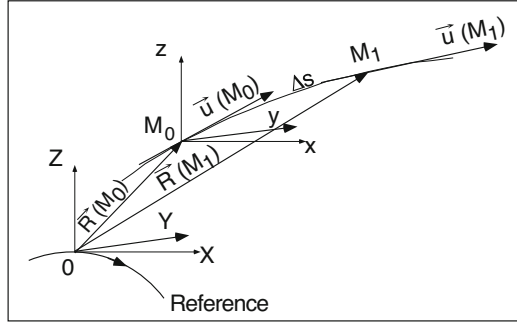
In order to integrate the Lorentz equation (m is the particle mass, q its charge, \mathbf{v} the velocity, \mathbf{e} and \mathbf{b} the local electric and magnetic fields)

$$\frac{d(\gamma m \mathbf{v})}{dt} = q (\mathbf{e} + \mathbf{v} \times \mathbf{b}) \quad (9.5)$$

we rewrite it by noting that $(\)' = \frac{d(\)}{ds}$, $\mathbf{u} = \frac{\mathbf{v}}{v}$, $ds = v dt$, $\gamma m \mathbf{v} = \gamma m v \mathbf{u} = q B \rho \mathbf{u}$, and $B \rho$ the rigidity of the particle,

$$(B\rho)' \mathbf{u} + B\rho \mathbf{u}' = \frac{\mathbf{e}}{v} + \mathbf{u} \times \mathbf{b}, \quad (9.6)$$

Fig. 9.2 Position and velocity of a particle in **Zgoubi** reference frame



Zgoubi uses truncated Taylor developments of the position \mathbf{R} and normalized velocity \mathbf{u} vectors, namely,

$$\begin{aligned} \mathbf{R}(M_1) &\approx \mathbf{R}(M_0) + \mathbf{u}(M_0) \Delta s + \mathbf{u}'(M_0) \frac{\Delta s^2}{2!} + \dots + \mathbf{u}''''(M_0) \frac{\Delta s^6}{6!} \\ \mathbf{u}(M_1) &\approx \mathbf{u}(M_0) + \mathbf{u}'(M_0) \Delta s + \mathbf{u}''(M_0) \frac{\Delta s^2}{2!} + \dots + \mathbf{u}''''(M_0) \frac{\Delta s^5}{5!} \end{aligned} \quad (9.7)$$

In these series $\mathbf{R}(M_0)$ and $\mathbf{u}(M_0)$ are the initial conditions, at point M_0 , $\mathbf{R}(M_1)$ and $\mathbf{u}(M_1)$ are one integration step Δs ahead, at point M_1 (Fig. 9.2). The rigidity varies in the presence of electric field, it is calculated the same way using

$$(B\rho)(M_1) \approx (B\rho)(M_0) + (B\rho)'(M_0) \Delta s + \dots + (B\rho)''''(M_0) \frac{\Delta s^5}{5!} \quad (9.8)$$

The time of flight is expanded in a similar manner

$$T(M_1) \approx T(M_0) + T'(M_0) \Delta s + T''(M_0) \frac{\Delta s^2}{2} + \dots + T''''(M_0) \frac{\Delta s^5}{5!} \quad (9.9)$$

which simplifies to $T(M_1) = T(M_0) + \Delta s/v$ in the absence of electric field.

The derivatives $\mathbf{u}^{(n)} = \frac{d^n \mathbf{u}}{ds^n}$ and $(B\rho)^{(n)} = \frac{d^n (B\rho)}{ds^n}$ involved in these expressions are calculated by recursive differentiation of Eq. 9.6, details can be found in the Users' Guide [16].

Spin in **Zgoubi** is evaluated in the same manner as the particle, with the three spin vector components treated independently. The T-BMT equation is recast as,

$$\frac{d\mathbf{S}}{dt} = \frac{q}{m\gamma} \mathbf{S} \times \boldsymbol{\omega} \quad (9.10)$$

with, in the laboratory frame,

$$\boldsymbol{\omega} = (1 + \gamma G)\mathbf{b} - G(\gamma - 1)\mathbf{b}_{\parallel} + \gamma(G + \frac{1}{1 + \gamma})\frac{\mathbf{e} \times \mathbf{v}}{c^2} \quad (9.11)$$

wherein \mathbf{b} and \mathbf{e} are the fields in the laboratory, \mathbf{b}_{\parallel} is the component of \mathbf{b} parallel to the velocity \mathbf{v} of the particle. Equation (9.10) is normalized by introducing again $v = \|\mathbf{v}\|$, $\mathbf{v} = v\mathbf{u}$, $ds = vdt$ the differential path, $\frac{\gamma mv}{q} = B\rho$ the rigidity of the particle, whereas $b = \|\mathbf{b}\|$, $\mathbf{S}' = \frac{d\mathbf{S}}{ds} = \frac{1}{v} \frac{d\mathbf{S}}{dt}$ is the derivative of the spin with respect to the path. This yields

$$(B\rho)\mathbf{S}' = \mathbf{S} \times \boldsymbol{\omega} \quad \text{or} \quad \mathbf{S}' = \mathbf{S} \times \boldsymbol{\Omega} \quad (9.12)$$

where, noting $\mathbf{B} = \mathbf{b}/B\rho$, $\mathbf{E} = \mathbf{e}/B\rho$,

$$\boldsymbol{\Omega} = \frac{\boldsymbol{\omega}}{B\rho} = (1 + \gamma G)\mathbf{B} + G(1 - \gamma)\mathbf{B}_{\parallel} + \frac{\beta\gamma}{c} \left(G + \frac{1}{1 + \gamma} \right) \mathbf{E} \times \mathbf{u} \quad (9.13)$$

From the initial conditions $\boldsymbol{\Omega}(M_0)$ and $\mathbf{S}(M_0)$ of the particle at position M_0 , the spin $\mathbf{S}(M_1)$ at position M_1 , following a displacement Δs (Fig. 9.2), is obtained from the truncated Taylor expansion

$$\mathbf{S}(M_1) \approx \mathbf{S}(M_0) + \mathbf{S}'(M_0) \Delta s + \mathbf{S}''(M_0) \frac{\Delta s^2}{2!} + \dots + \mathbf{S}''''(M_0) \frac{\Delta s^5}{5!} \quad (9.14)$$

The spin vector \mathbf{S} and its derivatives $\mathbf{S}^{(n)} = d^n \mathbf{S} / ds^n$ are obtained by recursive differentiation of Eq. 9.12, details in the Users' Guide [16].

9.4 SPINK

SPINK code was developed in the 1990s by Alfredo Luccio and used to extensively model the RHIC machine which was being built at the time. It employed the linear transport matrices from the MAD8 code to track the orbit, estimating the position of the charged particles inside each magnet and thus deducing the field. Beginning from the T-BMT equation:

$$\frac{d\mathbf{S}}{dt} = \frac{e}{\gamma m} \mathbf{S} \times \mathbf{F} \quad (9.15)$$

now with \mathbf{F} defined as (we now assume no electric field)

$$\mathbf{F} = (1 + G\gamma)\mathbf{B}_{\perp} + (1 + G)\mathbf{B}_{\parallel} \quad (9.16)$$

and with the perpendicular and parallel components of the magnet field expressed as,

$$\mathbf{B}_\perp = \frac{1}{v^2}(\mathbf{v} \times \mathbf{B}) \times \mathbf{v}, \quad \mathbf{B}_\parallel = \frac{1}{v^2}(\mathbf{v} \cdot \mathbf{B})\mathbf{v}, \quad (9.17)$$

\mathbf{F} can be expressed as,

$$\mathbf{F} = (1 + G\gamma)\mathbf{B} - G(\gamma - 1)\frac{1}{v^2}(\mathbf{v} \cdot \mathbf{B})\mathbf{v} \quad (9.18)$$

As discussed in previous sections the velocity vector can be expressed in terms of the derivative of the spatial coordinates with respect to the longitudinal coordinate s to obtain:

$$\mathbf{v} = \frac{d\mathbf{r}}{dt} = \left[x'\hat{\mathbf{x}} + y'\hat{\mathbf{y}} + \left(1 + \frac{x}{\rho}\hat{\mathbf{z}}\right) \frac{ds}{dt} \right] \quad (9.19)$$

One can now rewrite the T-BMT equation as an s derivative,

$$\frac{d\mathbf{S}}{ds} = \mathbf{S} \times \boldsymbol{\Omega} \quad (9.20)$$

with,

$$\boldsymbol{\Omega} = \frac{h}{B\rho} \left[(1 + G\gamma)\mathbf{B} - G(\gamma - 1)(\mathbf{r}' \cdot \mathbf{B})\mathbf{r}' \right] \quad (9.21)$$

and,

$$\begin{aligned} \frac{e}{\gamma m} &= \frac{v}{B\rho} & (9.22) \\ h &= \sqrt{x'^2 + y'^2 + \left(1 + x/\rho\right)^2} \\ \mathbf{r}' &= \frac{\mathbf{v}}{v}. \end{aligned}$$

Using this the T-BMT equation can be reduced to a third order differential equation,

$$\mathbf{S}''' + \omega(s)^2\mathbf{S}' = 0 \quad (9.23)$$

where,

$$\omega(s)^2 = \Omega_x(s)^2 + \left(\Omega_y(s) - \frac{1}{\rho(s)}\right)^2 + \Omega_z(s)^2 \quad (9.24)$$

In the case that both the fields and orbits are constant across a given portion of the magnet then $\omega(s)$ would likewise be constant and solutions in the form of transport matrices can be developed yielding,

$$\begin{pmatrix} 1 - (B^2 + C^2)c & ABc + Cs & ACc - Bs \\ ABc - Cc & 1 - (A^2 + C^2)c & BCc + As \\ ACc + Bs & BCc - As & 1 - (A^2 + B^2)c \end{pmatrix} \quad (9.25)$$

with

$$c = 1 - \cos \omega \delta s, s = \sin \omega \delta s \quad (9.26)$$

$$A = \frac{\Omega_x}{\omega}, B = \frac{\Omega_y - 1/\rho}{\omega}, C = \frac{\Omega_z}{\omega}$$

9.4.1 Bends

Applied to the case of the rectangular bend magnet with $B_x = B_z = 0$ and $B_y = B\rho/\rho$ one obtains the matrix,

$$\begin{pmatrix} \cos \delta\psi & 0 & \sin \delta\psi \\ 0 & 1 & 0 \\ -\sin \delta\psi & 0 & \cos \delta\psi \end{pmatrix}. \quad (9.27)$$

This represents a rotation about the vertical axis through an angle of,

$$\delta\psi = \omega \delta s = \left[G\gamma - (1 + G\gamma) \frac{x}{\rho} \right] \delta\theta \quad (9.28)$$

with $\delta\theta = \delta s/\rho$ the bend angle.

9.4.2 Quadrupoles

For the quadrupole with a gradient of k_1 the fields become $B_x = k_1 B\rho y$, $B_y = k_1 B\rho x$ and $B_z = 0$ with $\frac{1}{\rho} = 0$. In this case the transport matrix becomes,

$$\frac{1}{r^2} \begin{pmatrix} y^2 + x^2 \cos \delta\psi & xy(1 - \cos \delta\psi) & -xr \sin \delta\psi \\ xy(1 - \cos \delta\psi) & y^2 + x^2 \cos \delta\psi & yr \sin \delta\psi \\ xr \sin \delta\psi & -yr \sin \delta\psi & \cos \delta\psi \end{pmatrix} \quad (9.29)$$

with $\omega = k_1(1 + G\gamma)r$ and $r = \sqrt{x^2 + y^2}$

SPINK made use of the MAD8 generated Twiss functions to calculate the transport matrices and thus coordinates at the beginning and exit of each element. It takes the average of the position between the beginning and end of each sliced transport element to estimate the field that acts on the spin. The accuracy of the solution is controlled by increasing the number of slices in MAD8.

9.5 GPU SPIN TRACK

GPU SPIN TRACK was developed from a version of SPINK which uses a native teapot integrator called UAL-SPINK. It reads lattices formatted in the SXF style. The development of GPU SPIN TRACK was motivated by problems with convergence using the drift and thin kick style teapot orbit integrator. As a result a new orbit integrator was developed which is detailed in [11]. It was observed that when crossing strong spin resonance in the presence of snakes, the highly accurate rendering of the orbital trajectory through the quadrupoles was essential to achieve convergence with a reasonable number of slices.

9.5.1 How to Integrate the Quadrupole?

The Hamiltonian for quadrupole is given by,

$$H_Q = H_D(P_t, P_x, P_y) + H_K(X, Y) \quad (9.30)$$

$$H_D(P_t, P) = -\sqrt{1 + \frac{2}{\beta_0} P_t + P_t^2 - P_x^2 - P_y^2} + \frac{1}{\beta_0} P_t$$

$$H_K(X, Y) = \frac{k_1}{2} (X^2 - Y^2).$$

Here $P_t = \frac{\gamma - \gamma_0}{\beta_0 \gamma_0}$ with subscript 0 indicating on-momentum values for the relativistic gamma and beta and k_1 the quadrupole gradient. The usual teapot approach is to split this Hamiltonian into H_D for the drift and H_K for the kick. The effect of each of these pieces can be exactly evaluated yielding a drift transport matrix and a thin kick part. The drifts are then split in half and sandwiched around the thin kick. An improved approach which yields higher accuracy is to split the Hamiltonian in a different way, by adding and subtracting as follows,

$$H_M = \frac{1}{2} (P_x^2 + P_y^2) + \frac{k_1}{2} (X^2 - Y^2) \quad (9.31)$$

$$H_K = -\sqrt{1 + \frac{2}{\beta_0} P_t + P_t^2 - P_x^2 - P_y^2} + \frac{1}{\beta_0} P_t - \frac{1}{2} (P_x^2 + P_y^2)$$

Here we add and subtract $\frac{1}{2} (P_x^2 + P_y^2)$ from each term to create a matrix transport H_M . GPUSPINTRACK additionally divides the momentum term by the energy contribution to momentum to get the correct tunes for the off energy particles yielding,

$$H_M = \frac{1}{2} \frac{P_x^2 + P_y^2}{\sqrt{1 + \frac{2}{\beta_0} P_t + P_t^2}} + \frac{k_1}{2} (X^2 - Y^2) \tag{9.32}$$

$$H_K = -\sqrt{1 + \frac{2}{\beta_0} P_t + P_t^2 - P_x^2 - P_y^2} + \frac{1}{\beta_0} P_t - \frac{1}{2} \frac{P_x^2 + P_y^2}{\sqrt{1 + \frac{2}{\beta_0} P_t + P_t^2}}$$

9.5.2 Spin Precession Calculation

With the orbit the spin transport can be calculated across a given element slice as was done in the original SPINK code. However GPUSPINTRACK accelerates computation and the spin convergence by making use of Romberg quadrature with quaternions to represent the spin transport using SPINK Ω . The approach is to calculate the quaternions for $q(h\Omega)$ for different relative step sizes h across a given magnetic element as follows,

$$R_{0,2} = Q(h) = q\left(\frac{1}{2}h\Omega_4\right)q(h\Omega_3)q(h\Omega_2)q(h\Omega_1)q\left(\frac{1}{2}h\Omega_0\right) \tag{9.33}$$

$$R_{0,1} = Q(2h) = q(h\Omega_4)q(2h\Omega_2)q(h\Omega_0)$$

$$R_{0,0} = Q(4h) = q(2h\Omega_4)q(2h\Omega_0).$$

Here Ω_i represents the calculated spin precession vector at a given slice across the magnetic element (see Fig. 9.3). With this, one can construct a ‘bootstrapped’

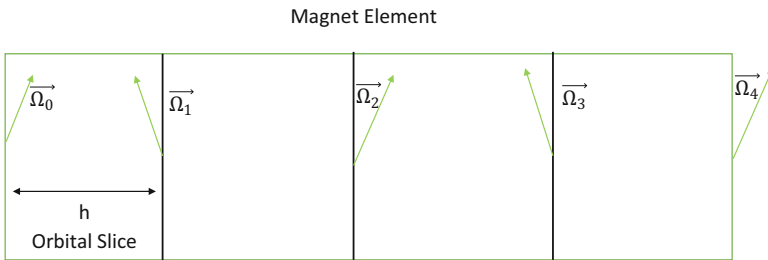


Fig. 9.3 Slicing up magnetic element for Romberg integration

quaternion across the whole element to arbitrary order using,

$$R_{j+1,k} = \frac{4^{j+1}R_{j,k} - R_{j,k-1}}{4^{j+1} - 1} \quad (9.34)$$

9.6 How to Integrate the T-BMT Equation by Hand

Aside from numerical integration, it is possible to integrate certain forms of it analytically. Beginning with Eq. 9.20 in the absence of solenoid magnets and vertical bends, the T-BMT equation can, to first order in the coordinates (x, s, z) , be rewritten as (see Exercise 1).

$$\begin{aligned} \frac{d\mathbf{S}}{ds} &\approx v \left(\frac{dt}{ds} \right) \mathbf{S} \times \boldsymbol{\Omega} \approx \mathbf{S} \times \boldsymbol{\Omega} \\ \Omega_x &= -(1 + G\gamma)z'' \\ \Omega_s &= (1 + G\gamma)z'/\rho - (1 + G) \left(\frac{z}{\rho} \right)' \\ \Omega_z &= x''(1 + G\gamma) - \frac{1 + G\gamma}{\rho} \end{aligned}$$

Further, Accounting for the derivatives of the x, s, z basis vectors of \mathbf{S} we can obtain,

$$\begin{aligned} \frac{dS_x}{ds} &= S_s(\Omega_z + 1/\rho) - \Omega_s S_z \\ \frac{dS_s}{ds} &= -S_x(\Omega_z + 1/\rho) + \Omega_x S_z \\ \frac{dS_z}{ds} &= S_x \Omega_s - \Omega_x S_s \end{aligned}$$

If we change to a basis vector which rotates with the beam $(\hat{e}_1, \hat{e}_2, \hat{e}_3)$ we obtain,

$$\begin{aligned} \frac{d\mathbf{S}}{ds} &= \boldsymbol{\omega} \times \mathbf{S}, \\ \omega_1 &= (1 + G\gamma)z'', \\ \omega_2 &= -(1 + G\gamma)z'/\rho + (1 + G) \left(\frac{z}{\rho} \right)', \\ \omega_3 &= -(1 + G\gamma)x'' + \frac{G\gamma}{\rho}. \end{aligned} \quad (9.35)$$

This can be further transformed by defining a two-component *spinor* Ψ such that the j -th component of the spin vector is given by

$$S_j = \langle \Psi | \sigma_j | \Psi \rangle = \Psi^\dagger \sigma_j \Psi. \quad (9.36)$$

Here Ψ denotes a classical vector with components u and d , which are related to the three components of \mathbf{S} by

$$\begin{aligned} S_1 &= u^* d + u d^* \\ S_2 &= -i(u^* d - u d^*) \\ S_3 &= |u|^2 - |d|^2. \end{aligned} \quad (9.37)$$

Using $\boldsymbol{\sigma} = (\sigma_x, \sigma_y, \sigma_z)$, the vector of the Pauli spin matrices, and $\zeta(s) = -\omega_1 + i\omega_2$, it is possible to show (see Exercise 2) that Eq. 9.35 can be transformed into,

$$\frac{d\Psi}{ds} = -\frac{i}{2}(\boldsymbol{\sigma} \cdot \boldsymbol{\omega})\Psi = -\frac{i}{2}H\Psi = -\frac{i}{2} \begin{pmatrix} \frac{G\gamma}{\rho} & -\zeta(s) \\ -\zeta(s)^* & -\frac{G\gamma}{\rho} \end{pmatrix} \Psi, \quad (9.38)$$

where we have dropped the first term in ω_3 , $-(1+G\gamma)x''$, since it is small compared to $G\gamma$.

Using the differential relation $d\theta = ds/\rho$, one may transform (9.38) so as to make θ the independent variable. Then, considering the effects of a *single* resonance, wherein $\zeta(\theta)$ becomes $\epsilon_K e^{-iK\theta}$, the T-BMT equation becomes

$$\frac{d\Psi}{d\theta} = -\frac{i}{2} \begin{pmatrix} G\gamma & -\epsilon_K e^{-iK\theta} \\ -\epsilon_K^* e^{iK\theta} & -G\gamma \end{pmatrix} \Psi. \quad (9.39)$$

If we assume $G\gamma = \text{constant}$, and transform the spinor equation (9.39) into the *resonance precessing frame* by defining

$$\Psi_K(\theta) = e^{\frac{i}{2}K\theta\sigma_z}\Psi(\theta). \quad (9.40)$$

one can obtain (see Exercise 3),

$$\frac{d\Psi_K}{d\theta} = \frac{i}{2} \begin{pmatrix} K - G\gamma & \epsilon_K \\ \epsilon_K^* & G\gamma - K \end{pmatrix} \Psi_K. \quad (9.41)$$

Since all the elements of the matrix are constant one can simply exponentiate the matrix directly to obtain an exact solution to the differential equation. In the case when $G\gamma$ is not constant, but linearly accelerating, a solution is still possible and ultimately yields the famous Froissart-Stora formula.

In the case when $G\gamma = G\gamma_0 + \alpha\theta$ we can transform the spinor equation into the spin precessing frame by defining,

$$\Psi(\theta) = e^{-\frac{i}{2}\int_0^\theta G\gamma(x)dx\sigma_3}\Psi_I(\theta) \quad (9.42)$$

to obtain,

$$\frac{d\Psi_I}{d\theta} = \frac{i}{2} \begin{pmatrix} 0 & \epsilon_K e^{i[(G\gamma_0 - K)\theta + \frac{1}{2}\alpha\theta^2]} \\ \epsilon_K^* e^{-i[(G\gamma_0 - K)\theta + \frac{1}{2}\alpha\theta^2]} & 0 \end{pmatrix} \Psi_I. \quad (9.43)$$

which can be transformed into an ordinary second order homogeneous differential equation,

$$\frac{d^2\Psi_I^\pm}{d\theta^2} \mp i\alpha\theta \frac{d\Psi_I^\pm}{d\theta} + \frac{|\epsilon_K|^2}{4} \Psi_I^\pm = 0 \quad (9.44)$$

which has confluent hyper-geometric functions as solutions. Using the asymptotic expressions of these functions it is possible to show that, in the limit of large $|\theta|$,

$$S_z = 2e^{-\frac{\pi|\epsilon_K|^2}{2\alpha}} - 1 \quad (9.45)$$

which is the famous Froissart-Stora formula.

9.7 Calculating Spin Resonances

One of the first codes to calculate the strength of the intrinsic and imperfection spin resonance strength was developed by Ruth and Courant in 1980 and is known as DEPOL [19]. This code calculates the expansion of $\zeta(s)$ by making use of the linear transport matrix to derive an exact solution to the elements of the quasi Fourier integral,

$$\epsilon_K = -\frac{1}{2\pi N_T} \int_0^{CN_T} \left[(1 + G\gamma)(z'' + \frac{iz'}{\rho}) - i\rho(1 + G)(\frac{z}{\rho})' \right] e^{iK\theta(s)} ds \quad (9.46)$$

Here C is the circumference of the ring. The number of turns N_T depends on the rationality of K . If K is an integer then $N_T = 1$; however if K is an irrational number then we normally would need an infinite number of turns to approximate the resonance strength. Decomposing the integral into a sum of integrals over each element we obtain,

$$\epsilon_K = \sum_{lattice} \frac{\epsilon_{K_m}}{N_T} \quad (9.47)$$

$$\epsilon_{K_m} = -\frac{1}{2\pi} \int_{s_1}^{s_2} \left[(1 + G\gamma)(z'' + \frac{iz'}{\rho}) - i\rho(1 + G)(\frac{z}{\rho})' \right] e^{iK\theta(s)} ds$$

Assuming that $1/\rho$ is a step function, constant in the element and zero just outside of the element, partial integration leads to an intermediate form,

$$\epsilon_{K_m} = \frac{1}{2\pi} \left[\frac{(1+K)(\chi_1+i)}{\rho} z_1 e^{iK\theta_1} + \frac{(1+K)(\chi_2-i)}{\rho} z_2 e^{iK\theta_2} - (1+K) \int_{s_1}^{s_2} z'' e^{iK\theta} ds - \frac{K}{\rho^2} (K-G) \int_{s_1}^{s_2} z e^{iK\theta} ds \right] \quad (9.48)$$

Here χ_i is the contribution due to edge focusing of the magnet and $z_i = z(s_i)$. Applying partial integration to the last two terms yields,

$$\epsilon_{K_m} = \frac{1}{2\pi} \left[\frac{(1+K)(\chi_1+i)}{\rho} z_1 e^{iK\theta_1} + \frac{(1+K)(\chi_2-i)}{\rho} z_2 e^{iK\theta_2} - (1+K) \left[\left(z_2' - \frac{iK}{\rho} z_2 \right) e^{iK\theta_2} - \left(z_1' - \frac{iK}{\rho} z_1 \right) e^{iK\theta_1} \right] + \left(\frac{K(K^2+G)}{\rho^2} \right) \int_{s_1}^{s_2} z e^{iK\theta} ds \right] \quad (9.49)$$

In the uncoupled case the last term can be evaluated exactly using the homogeneous equation $z'' = -K_z z$, where $K_z(s)$ is the focusing function of the guide field. Substitution and integration by parts yields,

$$\int_{s_1}^{s_2} z e^{iK\theta} ds = \frac{\left(z_2' - \frac{iK}{\rho} z_2 \right) e^{iK\theta_2} - \left(z_1' - \frac{iK}{\rho} z_1 \right) e^{iK\theta_1}}{K_z - K^2/\rho^2}. \quad (9.50)$$

DEPOL uses Courant-Snyder parameters from the MAD output files to construct the $z_{1,2}$ and $z'_{1,2}$ values. In calculating the resonance integral, one can factor out the phases which change with each period around the lattice. The remaining elements in the sum remain constant for each pass. This permits the evaluation of the integral over just one pass.

Later other more general algorithms have been developed to calculate spin resonances for arbitrary spin orientation [29]. Currently there exists the **SPRINT** [21] code which also can perform these calculations. As well an extension to the **DEPOL** algorithm was developed to handle resonance calculations in the case of linear betatron coupling. More recently the code **ASPIRRIN** [20] was developed to calculate spin resonances in the presence of snakes.

9.8 Integration of the Spinor T-BMT Equation for Many Resonances

In the case that one wants to include the effects of two resonances an analytical approximation has been derived [30], which makes use of the fact that the spinor form of the T-BMT equation can be expressed as a parametric oscillator. However these expressions are long and unwieldy. They do however permit the identification

of regions in θ where the system can be approximated using only the single dominant resonance outside of the parametric resonance tongues.

In the case that one has more than two resonances, then numerical methods should be used. The T-BMT c++ method performs this integration using a 4th order Magnus Gaussian quadrature. With the spinor T-BMT equation expressed compactly as,

$$\Psi' = \mathbf{A}(\theta)\Psi, \quad \Psi(\theta_0) = \Psi_0 \quad (9.51)$$

it evaluates $A(\theta)$ at two orbital locations $\theta + (\frac{1}{2} \pm \frac{\sqrt{3}}{6})h$ with step size h :

$$A_1 = A \left[\theta_n + \left(\frac{1}{2} - \frac{\sqrt{3}}{6} \right) h \right] \quad (9.52)$$

$$A_2 = A \left[\theta_n + \left(\frac{1}{2} + \frac{\sqrt{3}}{6} \right) h \right].$$

These are then used to calculate the Ω used to propagate the spinor:

$$\Omega^{[4]}(h) = \frac{h}{2}(A_1 + A_2) - h^2 \frac{\sqrt{3}}{12}[A_1, A_2] \quad (9.53)$$

$$\Psi_{n+1} = e^{\Omega^{[4]}(h)}\Psi_n$$

Here we use the identity,

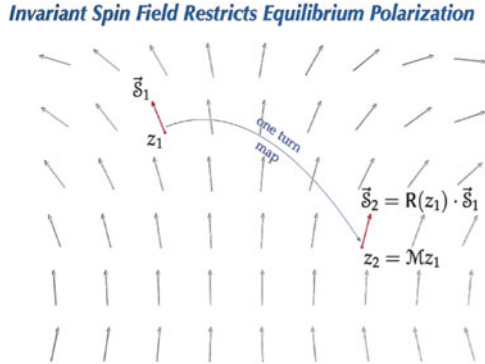
$$e^{i\mathbf{a}\cdot\boldsymbol{\sigma}} = \cos |a|I + i \sin |a| \frac{\mathbf{a} \cdot \boldsymbol{\sigma}}{|a|} \quad (9.54)$$

to generate the two-by-two complex matrix to transport the spinors. To reduce the number of integration steps necessary, the T-BMT code transforms first to the interaction frame before performing the 4th order Magnus Gaussian quadrature.

9.9 Initialization of Spinors

For any realistic spin tracking it is necessary to initialize the spinors to the invariant spin field (ISF) before tracking. For most lower energy machines the ISF trivially points vertically along the dominant dipole guide field. In these cases initialization involves setting the spinor to point vertically up or down. However at higher energies or with machines having more complex guide fields the ISF can assume a very complex and spread-out structure as shown in Fig. 9.4. If the spinors are not initially aligned with the ISF then they will execute a precession around the local ISF. This will make it appear that there is a spin resonance or depolarization mechanism when

Fig. 9.4 Structure of the Invariant Spin Field



in fact no polarization would be lost if the spins had been initially aligned with the ISF. Several approaches using stroboscopic averaging were developed by K. Heinemann and G.H.Hoffstatter [21]. T-BMT code and GPUSPINTRACK code employ one of the forward tracking methods detailed in this paper. Here three spin vectors each of which points along the $\hat{x} (= (1, 0, 0))$, $\hat{z} (= (0, 1, 0))$, and $\hat{s} (= (0, 0, 1))$ directions are tracked for each orbital phase space point. These are then tracked through one turn to establish the one turn spin transport matrix (\mathbf{R}_0), the eigenvector of which is calculated to give the spin closed orbit vector \hat{n}_0 . This is then dotted into subsequent transport matrices \mathbf{R}_n each turn and accumulated in a total vector \mathbf{b} ,

$$\mathbf{b}_{n+1} = \mathbf{b}_n + \mathbf{R}_n \cdot \hat{n}_0. \tag{9.55}$$

which is then averaged and normalized to yield the ISF for each phase space point which we want to track. One then needs to select an appropriate number of turns to achieve convergence to the ISF. The number of turns depends on one's proximity to a resonance and the overall nature of the ISF. Evidence that one has not converged can be seen in the turn-by-turn precession of the spin vector for a particle which is not aligned with the ISF.

9.10 Homework

? Exercise 1

Show that in the absence of solenoid magnets and vertical bends, the T-BMT equation can, to first order in the coordinates (x, s, z) , be rewritten as

$$\frac{d\mathbf{S}}{ds} \approx v \left(\frac{dt}{ds} \right) \mathbf{S} \times \boldsymbol{\Omega} \approx \mathbf{S} \times \boldsymbol{\Omega}$$

$$\begin{aligned}\Omega_x &= -(1 + G\gamma)z'' \\ \Omega_s &= (1 + G\gamma)z'/\rho - (1 + G)\left(\frac{z}{\rho}\right)' \\ \Omega_z &= x''(1 + G\gamma) - \frac{1 + G\gamma}{\rho}\end{aligned}$$

Here you will use the fact that $B\rho = \gamma mv/e$ and approximate $\frac{dt}{ds} \approx 1/v$ since the other terms will introduce orders of x, s, z and $1/\rho$ beyond our approximation. To accomplish this you will also need to first express the perpendicular and parallel magnetic field components in the forms

$$\mathbf{B}_\perp = \frac{1}{v^2}(\mathbf{v} \times \mathbf{B}) \times \mathbf{v}, \quad \mathbf{B}_\parallel = \frac{1}{v^2}(\mathbf{v} \cdot \mathbf{B})\mathbf{v}. \quad (9.56)$$

Then use the Lorentz force equation to express $\mathbf{v} \times \mathbf{B}$, hence also \mathbf{B}_\perp in terms of $d\mathbf{v}/dt$:

$$\frac{d\mathbf{v}}{dt} = \frac{q}{m\gamma} \mathbf{v} \times \mathbf{B}, \quad (9.57)$$

$$\mathbf{B}_\perp = \frac{m\gamma}{qv^2} \frac{d\mathbf{v}}{dt} \times \mathbf{v}. \quad (9.58)$$

In addition, make use of the fact that

$$\frac{ds}{dt} = \frac{v}{\left[\left(1 + \frac{x}{\rho}\right)^2 + x'^2 + z'^2\right]^{1/2}}, \quad (9.59)$$

where ρ denotes the radius of curvature of the local Frénet-Serret coordinate system.

Solution

The solution involves using 9.2 together with 9.56 through 9.59 in the T-BMT equation 9.1 to obtain the first-order result 9.56. In the present context, “first-order” means drop all terms of second order and higher in $x, z, 1/\rho$ and their derivatives. Also remember to make use of the initial assumption that solenoids and vertical bends are absent.

You also need to use the fact that the vertical field can be approximated using the strength of the dipole guide field, $B_z \approx -\frac{[B\rho]}{\rho}$. The longitudinal field can be approximated using Ampere’s law and assuming that $B_s(z=0) = 0$.

$$\frac{\partial B_s}{\partial z} = \frac{\partial B_z}{\partial s} = -B\rho \left(\frac{1}{\rho}\right)' \quad (9.60)$$

Accounting for the derivatives of the x, s, z basis vectors of \mathbf{S} we can obtain,

$$\begin{aligned}\frac{dS_x}{ds} &= S_s(\Omega_z + 1/\rho) - \Omega_s S_z \\ \frac{dS_s}{ds} &= -S_x(\Omega_z + 1/\rho) + \Omega_x S_z \\ \frac{dS_z}{ds} &= S_x \Omega_s - \Omega_x S_s\end{aligned}$$

If we change to a basis vector which rotates with the beam ($\hat{e}_1, \hat{e}_2, \hat{e}_3$) we obtain,

$$\begin{aligned}\frac{d\mathbf{S}}{ds} &= \mathbf{f} \times \mathbf{S}, \\ f_1 &= (1 + G\gamma)z'', \\ f_2 &= -(1 + G\gamma)z'/\rho + (1 + G)\left(\frac{z}{\rho}\right)', \\ f_3 &= -(1 + G\gamma)x'' + \frac{G\gamma}{\rho}.\end{aligned}\tag{9.61}$$

More formally, we can use the following derivation steps, neglecting solenoid magnets and vertical bends.

$$\mathbf{B}_\perp = \frac{(\mathbf{v} \times \mathbf{B}) \times \mathbf{v}}{v^2}\tag{9.62}$$

Using the Lorentz force equation we can express $\mathbf{v} \times \mathbf{B}$ as:

$$\frac{d\mathbf{v}}{dt} = \frac{e}{\gamma m} \mathbf{v} \times \mathbf{B}\tag{9.63}$$

$$\mathbf{B}_\perp = \frac{1}{v^2} \frac{m\gamma}{e} \frac{d\mathbf{v}}{dt} \times \mathbf{v}\tag{9.64}$$

Now expressing \mathbf{v} and its derivative in terms of its coordinates we get,

$$\frac{d\mathbf{v}}{dt} = \frac{d}{dt} \left[\frac{d\mathbf{r}}{dt} \right]\tag{9.65}$$

$$\frac{d\mathbf{r}}{dt} = \frac{ds}{dt} \frac{d\mathbf{r}}{ds}\tag{9.66}$$

$$\begin{aligned}\mathbf{v} &= \frac{ds}{dt} \left(\frac{dr_0(s)}{ds} + \frac{dx}{ds} \hat{x} + s \frac{d\hat{x}}{ds} + \frac{dz}{ds} \hat{z} + z \frac{d\hat{z}}{ds} \right) \\ &= \frac{ds}{dt} \left((1 + x/\rho) \hat{s} + x' \hat{x} + z' \hat{z} \right)\end{aligned}\tag{9.67}$$

$$\begin{aligned}
\frac{d\mathbf{v}}{dt} &= \left(\frac{ds}{dt}\right)^2 \frac{d}{ds} \left[\left(1 + x/\rho\right) \hat{s} + x' \hat{x} + z' \hat{z} \right] \\
&= \left(\frac{ds}{dt}\right)^2 \left[\left(\frac{2x'}{\rho} + x \left(\frac{1}{\rho}\right)' \right) \hat{s} + \right. \\
&\quad \left. \left(x'' - \frac{1}{\rho} - \frac{x}{\rho^2} \right) \hat{x} + z'' \hat{z} \right]
\end{aligned} \tag{9.68}$$

Now calculating the cross product,

$$\begin{aligned}
\frac{d\mathbf{v}}{dt} \times \mathbf{v} &= \left(\frac{ds}{dt}\right)^3 \left[\hat{x} \left[\left(\frac{2x'}{\rho} - x \left(\frac{1}{\rho}\right)' \right) z' - \left(1 + \frac{x}{\rho}\right) z'' \right] \right. \\
&\quad - \hat{s} \left[z' \left(x'' - \frac{1}{\rho} - \frac{x}{\rho^2} \right) - x' z'' \right] \\
&\quad + \hat{z} \left[\left(x'' - \frac{1}{\rho} - \frac{x}{\rho^2} \right) \left(1 + \frac{x}{\rho}\right) - \right. \\
&\quad \left. x' \left(\frac{2x'}{\rho} + x \left(\frac{1}{\rho}\right)' \right) \right] \Big] \\
&\approx \left(\frac{ds}{dt}\right)^3 \left[-\hat{x} z'' + \hat{s} \frac{z'}{\rho} + \hat{z} \left(x'' - \frac{1}{\rho} \right) \right]
\end{aligned} \tag{9.69}$$

Where at the last step we drop all terms higher than second order in x , z , s and $1/\rho$ and their derivatives. The expression for \mathbf{B}_\perp becomes,

$$\begin{aligned}
\mathbf{B}_\perp &\approx \frac{m\gamma v}{e} \frac{\left[-\hat{x} z'' + \hat{s} \frac{z'}{\rho} + \hat{z} \left(x'' - \frac{1}{\rho} \right) \right]}{\left[\left(1 + \frac{x}{\rho}\right)^2 + x'^2 + z'^2 \right]^{3/2}} \\
&\approx \frac{m\gamma v}{e} \left[-\hat{x} z'' + \hat{s} \frac{z'}{\rho} + \hat{z} \left(x'' - \frac{1}{\rho} \right) \right].
\end{aligned} \tag{9.70}$$

Here the denominator goes to 1 when we drop all the second order terms in x , z , s and $1/\rho$ and their derivatives. We also used the fact that,

$$\frac{ds}{dt} = \frac{v}{\left[\left(1 + \frac{x}{\rho}\right)^2 + x'^2 + z'^2 \right]^{1/2}}. \tag{9.71}$$

For the parallel field we get,

$$\begin{aligned}
 \mathbf{B}_{\parallel} &= \frac{(\mathbf{v} \cdot \mathbf{B}) \mathbf{v}}{v^2} \\
 &= \frac{\left(\frac{ds}{dr}\right)^2}{v^2} \left[\left(1 + \frac{x}{\rho}\right) B_s + x' B_x + z' B_z \right] \left[\left(1 + \frac{x}{\rho}\right) \hat{s} \right. \\
 &\quad \left. + x' \hat{x} + z' \hat{z} \right] \\
 &= \frac{\left[\left(1 + \frac{x}{\rho}\right) B_s + x' B_x + z' B_z \right] \left[\left(1 + \frac{x}{\rho}\right) \hat{s} + x' \hat{x} + z' \hat{z} \right]}{\left[\left(1 + \frac{x}{\rho}\right)^2 + x'^2 + z'^2 \right]} \\
 &\approx \left(1 - 2\frac{x}{\rho}\right) \left[\hat{s} \left(B_s + 2\frac{x}{\rho} B_s + x' B_x + z' B_z \right) + \right. \\
 &\quad \left. \hat{x} x' B_s + \hat{z} z' B_s \right] \\
 &\approx (B_s + z' B_z) \hat{s}
 \end{aligned} \tag{9.72}$$

Here the first approximation involves dropping terms x, z, s and $1/\rho$ and their derivatives to second order and above. The second approximation involves assumptions of the relative magnitude of B_s and $z' B_z$ to be $\gg B_s x/\rho, x' B_x, z' B_s$. This assumes no solenoid type magnets. The vertical field can be approximated using the strength of the dipole guide field, $B_z \approx -\frac{[B\rho]}{\rho}$. The longitudinal field can be approximated using Ampere's law and assuming that $B_s(z=0) = 0$.

$$\begin{aligned}
 \frac{\partial B_s}{\partial z} &= \frac{\partial B_z}{\partial s} = -B\rho \left(\frac{1}{\rho}\right)' \\
 B_s &= -B\rho z \left(\frac{1}{\rho}\right)' \hat{s} \\
 \mathbf{B}_{\parallel} &\approx \left(-B\rho z \left(\frac{1}{\rho}\right)' + \frac{z'}{\rho} B\rho \right) \hat{s} = -B\rho \left(\frac{z}{\rho}\right)' \hat{s}
 \end{aligned} \tag{9.73}$$

Putting this into the T-BMT equation we obtain,

$$\begin{aligned}
 \frac{d\mathbf{S}}{ds} &\approx v \left(\frac{dt}{ds}\right) \mathbf{S} \times \boldsymbol{\Omega} \approx \mathbf{S} \times \boldsymbol{\Omega} \\
 \Omega_x &= -(1 + G\gamma) z'' \\
 \Omega_s &= (1 + G\gamma) z'/\rho - (1 + G) \left(\frac{z}{\rho}\right)' \\
 \Omega_z &= x''(1 + G\gamma) - \frac{1 + G\gamma}{\rho}
 \end{aligned}$$

Here we used $B\rho = \gamma mv/e$ and approximate $\frac{dt}{ds} \approx 1/v$ since the other terms will introduce orders of x, s, z and $1/\rho$ beyond our approximation. Accounting for the derivatives of the x, s, z basis vectors of \mathbf{S} we can obtain,

$$\begin{aligned}\frac{dS_x}{ds} &= S_s(\Omega_z + 1/\rho) - \Omega_s S_z \\ \frac{dS_s}{ds} &= -S_x(\Omega_z + 1/\rho) + \Omega_x S_z \\ \frac{dS_z}{ds} &= S_x \Omega_s - \Omega_x S_s\end{aligned}$$

If we change to a basis vector which rotates with the beam ($\hat{e}_1, \hat{e}_2, \hat{e}_3$) we obtain,

$$\begin{aligned}\frac{d\mathbf{S}}{ds} &= \mathbf{f} \times \mathbf{S} \\ f_1 &= -\Omega_x = (1 + G\gamma)z'' \\ f_2 &= -\Omega_s = -(1 + G\gamma)z'/\rho + (1 + G)\left(\frac{z}{\rho}\right)' \\ f_3 &= -(\Omega_z + 1/\rho) = -x''(1 + G\gamma) + \frac{G\gamma}{\rho}\end{aligned}\tag{9.74}$$

? Exercise 2

Define a two-component *spinor* Ψ such that the j -th component of the spin vector is given by

$$S_j = \langle \Psi | \sigma_j | \Psi \rangle = \Psi^\dagger \sigma_j \Psi.\tag{9.75}$$

Here Ψ denotes a classical vector with components u and d , which are related to the three components of \mathbf{S} by

$$\begin{aligned}S_1 &= u^* d + u d^* \\ S_2 &= -i(u^* d - u d^*) \\ S_3 &= |u|^2 - |d|^2.\end{aligned}\tag{9.76}$$

Using $\boldsymbol{\sigma} = (\sigma_x, \sigma_y, \sigma_z)$, the vector of the Pauli spin matrices, and $\zeta(s) = -\omega_1 + i\omega_2$, show that Eq. 9.61 can be transformed into,

$$\frac{d\Psi}{ds} = -\frac{i}{2}(\boldsymbol{\sigma} \cdot \mathbf{f})\Psi = -\frac{i}{2}H\Psi = -\frac{i}{2} \begin{pmatrix} \frac{G\gamma}{\rho} & -\zeta(s) \\ -\zeta(s)^* & -\frac{G\gamma}{\rho} \end{pmatrix} \Psi, \quad (9.77)$$

where we have dropped the first term in ω_3 , $-(1+G\gamma)x''$, since it is small compared to $G\gamma$.

Solution

$$\frac{d\mathbf{S}}{ds} = \mathbf{f} \times \mathbf{S} \quad (9.78)$$

$$\mathbf{S} = \Psi^\dagger \boldsymbol{\sigma} \Psi \quad (9.79)$$

$$\begin{aligned} \mathbf{S}' &= \Psi'^\dagger \boldsymbol{\sigma} \Psi + \Psi^\dagger \boldsymbol{\sigma} \Psi' \\ &= \mathbf{f} \times (\Psi^\dagger \boldsymbol{\sigma} \Psi) = \Psi^\dagger (\mathbf{f} \times \boldsymbol{\sigma}) \Psi \\ &= -\frac{i}{2} \Psi^\dagger [(\boldsymbol{\sigma} \cdot \mathbf{f})(\boldsymbol{\sigma}) - (\boldsymbol{\sigma})(\boldsymbol{\sigma} \cdot \mathbf{f})] \Psi \end{aligned} \quad (9.80)$$

where we used the identity $[\boldsymbol{\sigma} \cdot \mathbf{f}, \boldsymbol{\sigma}] = 2i(\mathbf{f} \times \boldsymbol{\sigma})$. We can then identify that

$$\Psi' = -\frac{i}{2}(\boldsymbol{\sigma} \cdot \mathbf{f})\Psi \quad (9.81)$$

? Exercise 3

Using the differential relation $d\theta = ds/\rho$, one may transform 9.77 so as to make θ the independent variable. Then, considering the effects of a *single* resonance, wherein $\zeta(\theta)$ becomes $\epsilon_K e^{-iK\theta}$, the T-BMT equation becomes

$$\frac{d\Psi}{d\theta} = -\frac{i}{2} \begin{pmatrix} G\gamma & -\epsilon_K e^{-iK\theta} \\ -\epsilon_K^* e^{iK\theta} & -G\gamma \end{pmatrix} \Psi. \quad (9.82)$$

At this point, assume $G\gamma = \text{constant}$, and transform the spinor equation 9.82 into the *resonance precessing frame* by defining

$$\Psi_K(\theta) = e^{\frac{i}{2}K\theta\sigma_z} \Psi(\theta). \quad (9.83)$$

Show that

$$\frac{d\Psi_K}{d\theta} = \frac{i}{2} \begin{pmatrix} K - G\gamma & \epsilon_K \\ \epsilon_K^* & G\gamma - K \end{pmatrix} \Psi_K. \quad (9.84)$$

Solution

$$\Psi = \begin{pmatrix} e^{-\frac{iK\theta}{2}} & 0 \\ 0 & e^{\frac{iK\theta}{2}} \end{pmatrix} \Psi_K \quad (9.85)$$

$$\Psi_K = \begin{pmatrix} e^{\frac{iK\theta}{2}} & 0 \\ 0 & e^{-\frac{iK\theta}{2}} \end{pmatrix} \Psi \quad (9.86)$$

$$\Psi'_K = \frac{iK}{2} \begin{pmatrix} e^{\frac{iK\theta}{2}} & 0 \\ 0 & -e^{-\frac{iK\theta}{2}} \end{pmatrix} \Psi + \begin{pmatrix} e^{\frac{iK\theta}{2}} & 0 \\ 0 & e^{-\frac{iK\theta}{2}} \end{pmatrix} \Psi' \quad (9.87)$$

$$\Psi'_K = \frac{iK}{2} \begin{pmatrix} e^{\frac{iK\theta}{2}} & 0 \\ 0 & -e^{-\frac{iK\theta}{2}} \end{pmatrix} \Psi - \frac{i}{2} \begin{pmatrix} e^{\frac{iK\theta}{2}} & 0 \\ 0 & e^{-\frac{iK\theta}{2}} \end{pmatrix} \begin{pmatrix} G\gamma & -\epsilon_K e^{-iK\theta} \\ -\epsilon_K^* e^{iK\theta} & -G\gamma \end{pmatrix} \Psi. \quad (9.88)$$

$$\begin{aligned} \Psi'_K &= \frac{iK}{2} \begin{pmatrix} e^{\frac{iK\theta}{2}} & 0 \\ 0 & -e^{-\frac{iK\theta}{2}} \end{pmatrix} \begin{pmatrix} e^{-\frac{iK\theta}{2}} & 0 \\ 0 & e^{\frac{iK\theta}{2}} \end{pmatrix} \Psi_K \\ &\quad - \frac{i}{2} \begin{pmatrix} e^{\frac{iK\theta}{2}} & 0 \\ 0 & -e^{-\frac{iK\theta}{2}} \end{pmatrix} \begin{pmatrix} G\gamma & -\epsilon_K e^{-iK\theta} \\ -\epsilon_K^* e^{iK\theta} & -G\gamma \end{pmatrix} \begin{pmatrix} e^{-\frac{iK\theta}{2}} & 0 \\ 0 & e^{\frac{iK\theta}{2}} \end{pmatrix} \Psi_K. \end{aligned} \quad (9.89)$$

$$\Psi'_K = \frac{i}{2} \begin{pmatrix} K & 0 \\ 0 & -K \end{pmatrix} \Psi_K - \frac{i}{2} \begin{pmatrix} G\gamma & -\epsilon_K \\ -\epsilon_K^* & -G\gamma \end{pmatrix} \Psi_K. \quad (9.90)$$

$$\Psi'_K = \frac{i}{2} \begin{pmatrix} K - G\gamma & \epsilon_K \\ \epsilon_K^* & G\gamma - K \end{pmatrix} \Psi_K. \quad (9.91)$$

? Exercise 4

The code `SpinTrack.cc` also known as T-BMT, integrates the single-resonance T-BMT equation 9.84 with two orthogonal snakes located at $\theta = 0$

Table 9.1 T-BMT code's input file Resonance.in

```

k0:      452
w0R,w0I: 0.0  0.0
k1:      453
w1R,w1I: 0.0  0.0
k2:      393
w2R,w2I: 0.432733  0.112896
k3:      392
w3R,w3I: 0.0  0.0
k4:      394
w4R,w4I: 0.0  0.0
k5:      422
w5R,w5I: 0.0  0.0
k6:      423
w6R,w6I: 0.0  0.0

```

and $\theta = \pi$, with an axis of rotation oriented at angle $\phi = \pm\pi/4$, as is the case in RHIC [31]. The code takes as input the file Resonance.in (Table 9.1 [31]).

In this version of the code, we integrate the single-resonance T-BMT equation by taking the matrix exponential of Eq. 9.84. In this case, our single resonance is located at $K = k_2 = 393 + Q_y = 422.67$ ($Q_y = 29.67$), with *strength* $\epsilon_K = 0.432733 + i0.112896$. The code's default initial value for $G\gamma_0$ is 414.8, with an acceleration rate of $\frac{dG\gamma}{d\theta} = 3.74118 \times 10^{-6} \text{ rad}^{-1}$ (as in RHIC). The default number of turns is $NT = 670,000$.

- With Resonance.in in your directory, run the code using:

```
mpirun -n 1 ./SpinTrack.out
```

This will generate a file called:

```
TBTamp1.000Tau5.000Qs8.900CV2.00Q29.670R0.dat
```

After some header information, it lists the turn number, value of $G\gamma$, vertical component of the spin vector S_y , and the estimated Envelope of the Spin vector given by the following equation:

$$\begin{aligned}
 \delta &= K - G\gamma \\
 \lambda &= \sqrt{\delta^2 + |\epsilon_k|^2} \\
 b &= \frac{|\epsilon_k|}{\lambda} \sin \frac{\lambda\pi}{2} \\
 S_{\text{env}} &= 1 - 8b^2(1 - b^2)
 \end{aligned} \tag{9.92}$$

Identify the locations of the nodes and anti-nodes.

- Now run the same code using the command

```
mpirun -n 1 ./SpinTrack.out \
  nstrobe= 1 Ggam0= 420.0 NT= 250000
```


In this case, you are now starting around an anti-node and turning off stroboscopic averaging to orient your initial spin vector. What is different about this tracking? How do you think you could compute the final polarization in this case?

- Run it again turning back on stroboscopic averaging by using:

```
mpisexec -n 1 ./SpinTrack.out Ggam0= 420.0 NT=
250000
```

How does the spin vector behave now?

- Run the code again, now using more particles:

```
mpisexec -n 20 ./SpinTrack.out Ggam0= 420.0 NT= 250000
```

Now the code should produce 20 files one for each particle where the complex phase of the spin resonance is distributed evenly over 0 to 2π . The “R0”, “R1” indicate the particle number for each file. The python script AvgFiled.py lists all the TBT*.dat files in the current directory and then reads them in calculating an average for the vertical Spin component. Run it using:

```
python AvgFiled.py > YourFileName.dat
```

It generates a file listing turn number, $G\gamma$, and average vertical Spin. Notice how the average trajectory converges.

References

1. E. Grorud, J.L. Laclare, G. Leleux, Résonances de dépolarisation dans Saturne 2 - Traitement par Ordinateur (Appendix B). Int. Rep. GOC-GERMA 75-48/TP-28, Saturne, CEA Saclay (24 juillet 1975)
2. A. Chao, Evaluation of radiative spin polarization in an electron storage ring. SLAC-PUB-2564 (July 1980). <https://inspirehep.net/files/e1af98d473d259c96fcd0aea6c7f8519>
3. F. Méot, A Numerical method for combined spin tracking and ray tracing of charged particles. Nucl. Instrum. Methods A **313**, 492–500 (1992). [https://doi.org/10.1016/0168-9002\(92\)90829-S](https://doi.org/10.1016/0168-9002(92)90829-S)
4. Integration of Thomas-BMT equation was introduced in Raytrace [23] in 1986, by N. Tsoupas, BNL, together with the handling of magnetic field maps, in the context of polarized beam and partial snake developments at the AGS. This allowed for instance to use the AGS main magnet measured field maps and track spins in their stray field along the extraction line to RHIC collider
5. Capabilities of a series of accelerator codes, including spin, as inventoried in: Los Alamos Accelerator Group: Computer Codes for Particle Accelerator Design and Analysis; A Compendium. LA-UR-90-1766 (May 1990), seem to be subject to some maintenance in: https://en.wikipedia.org/wiki/Accelerator_physics_codes#cite_note-1
6. F. Zimmermann et al., Accelerator physics code WEB repository, in *Proceedings of EPAC 2006, Edinburgh, Scotland*. <https://accelconf.web.cern.ch/e06/PAPERS/WEPCH141.PDF> Code collection: https://oraweb.cern.ch/pls/hhh/code_website.disp_allcat
7. D. Sagan, A relativistic charged particle simulation library. Nucl. Instrum. Methods A **558**, 356–359 (2006). <https://www.classe.cornell.edu/bmad/>
8. M. Berz, Computational aspects of design and simulation: COSY infinity. Nucl. Instrum. Methods A **298**, 473 (1990). <http://www.cosyinfinity.org/>

9. V. Balandin, Computation and analysis of spin dynamics, in *AIP Conference Proceedings*, vol. 391, issue 1. <https://doi.org/10.1063/1.52350>
10. A. Lehrach, Project overview and computational needs to measure electric dipole moments at storage rings. Proceedings of ICAP2012, Rostock-Warnemünde, Germany - MOAAI1. <https://accelconf.web.cern.ch/ICAP2012/papers/moaai1.pdf>
11. D.T. Abell, D. Meiser, V.H. Ranjbar, D.P. Barber, Accurate and efficient spin integration for particle accelerators. *Phys. Rev. ST Accel. Beams* **18**, 024001 (2015). <https://doi.org/10.1103/PhysRevSTAB.18.024001>. [arXiv:1501.03450 [physics.acc-ph]]
12. J. Kewisch, Simulation of electron spin depolarization with the computer code SITROS. DESY-83-032 (1983)
13. C. Montag, eRHIC DESIGN UPDATE. NAPAC2019, Lansing, MI, USA - MOYBA4. <https://accelconf.web.cern.ch/napac2019/papers/moyba4.pdf>
14. A.U. Luccio, F. Lin, New formalism in the spin tracking code spink, in *EPAC08 Conf. Proc. TUPP097* (2008)
15. M. Vogt, Bounds on the maximum attainable equilibrium spin polarization of protons in HERA. DESY-THESIS-2000-054 (Dec. 2000)
16. F. Méot, The ray-tracing code Zgoubi - status. *NIM A* **767**, 112–125 (2014); Méot, F.: Zgoubi Users' Guide. <https://sourceforge.net/p/zgoubi/code/HEAD/tree/trunk/guide/Zgoubi.pdf> Source code: <https://sourceforge.net/projects/zgoubi/files/>
17. A. Chao, SLIM: an early work revisited. *Conf. Proc. C* **0806233**, thppgm04 (2008). EPAC08-THPPGM04
18. V.H. Ranjbar, Calculating the polarization lifetime from the Thomas-Bargmann-Michel-Telegdi equation. *Phys. Rev. Accel. Beams* **22**(9), 091001 (2019). <https://doi.org/10.1103/PhysRevAccelBeams.22.091001>
19. E.D. Courant, R.D. Ruth, The acceleration of polarized protons in circular accelerators. BNL 51270, Brookhaven National Laboratory (September 12, 1980)
20. V. Ptitsyn, S.R. Mane, Yu. M. Shatunov, *Nucl. Instrum. Methods A* **608**, 225 (2009)
Yu.M. Shatunov, S.R. Mane, Calculations of spin response functions in rings with Siberian Snakes and spin rotators. *Phys. Rev. Spec. Top. Acceler. Beams* **12**, 024001 (2009)
21. K. Heinemann, G.H. Hoffstaetter, A Tracking algorithm for the stable spin polarization field in storage rings using stroboscopic averaging. *Phys. Rev. E* **54**, 4240–4255 (1996). <https://doi.org/10.1103/PhysRevE.54.4240>. [arXiv:acc-physics/9605001 [physics.acc-ph]]
22. F.T. Cole, O Camelot ! A memoir of the MURA years (April 1, 1994). <https://epaper.kek.jp/c01/cyc2001/extra/Cole.pdf>
23. S. Kowalski, H.A. Enge, The ion-optical program RAYTRACE. *Nucl. Instr. Methods A* **258**, 407 (1987)
24. F. Méot, Spin code benchmarking at RHIC, in *THP103, Proceedings of 2011 Particle Accelerator Conference, New York, NY, USA*. <https://accelconf.web.cern.ch/PAC2011/papers/thp103.pdf>
P. Adams et al., Numerical simulation of spin dynamics with spin flipper in RHIC. MOPMF018, IPAC2018, Vancouver, BC, Canada. <https://accelconf.web.cern.ch/ipac2018/papers/mopmf018.pdf>
25. Y. Duthiel, Spin dynamics modeling in the AGS based on a stepwise ray-tracing method. PhD Thesis Dissertation, BNL (April 2014)
26. K. Hock, Transport of Polarized helions in Injector Synchrotrons for the future electron-ion collider project at the Brookhaven National Laboratory. PhD Thesis Dissertation, BNL (Oct. 2021)
27. F. Méot, V. Ranjbar, Simulation of Polarized Electron Bunch Acceleration in EIC RCS. Bunch and Spin Densities at Extraction. BNL-219926-2020-TECH EIC-ADD-TN-007. <https://technotes.bnl.gov/PDF?publicationId=219926>
28. F. Méot, An ergodic approach to polarization in eRHIC electron storage ring. BNL-209351-2018-TECH. EIC/59 (Oct. 2018). <https://technotes.bnl.gov/PDF?publicationId=209351>
29. G.H. Hoffstaetter, Polarized protons in HERA. *Nucl. Phys. A* **666**, 203–213 (2000). [https://doi.org/10.1016/S0375-9474\(00\)00029-4](https://doi.org/10.1016/S0375-9474(00)00029-4). [arXiv:physics/0006007 [physics]]

30. V.H. Ranjbar, Approximations for crossing two nearby spin resonances. Phys. Rev. ST Accel. Beams **18**(1), 014001 (2015). <https://doi.org/10.1103/PhysRevSTAB.18.014001>
31. Exercise 4, code “SpinTrack.cc”, input file “ Resonance.in”, and Python script “AvgFiled.py” are available here: <https://uspas.fnal.gov/materials/21onlineSBU/Spin-Dynamics/Home-work/Spin-Codes/Code.shtml>

Open Access This chapter is licensed under the terms of the Creative Commons Attribution 4.0 International License (<http://creativecommons.org/licenses/by/4.0/>), which permits use, sharing, adaptation, distribution and reproduction in any medium or format, as long as you give appropriate credit to the original author(s) and the source, provide a link to the Creative Commons license and indicate if changes were made.

The images or other third party material in this chapter are included in the chapter’s Creative Commons license, unless indicated otherwise in a credit line to the material. If material is not included in the chapter’s Creative Commons license and your intended use is not permitted by statutory regulation or exceeds the permitted use, you will need to obtain permission directly from the copyright holder.

